Reducing motion artifacts in 4D CT image using principal component analysis combined with linear polynomial fitting model

Guangpu Shao [a], Xiaokun Hu [b], Jimin Yang and Juan Yang [*]

School of Physics and Electronics, Shandong Normal University, Jinan, China

[a]guangpushao@hotmail.com, [b]529512319@qq.com

[*] Corresponding author's e-mail: juan.yang@sdnu.edu.cn

Keywords: 4d ct,pca, linear polynomial fitting, dvfs.

Abstract: We propose a mathematical approach to reduce irregular artifacts in 4d ct images by fitting the generated displacement vector field (dvfs) from deformable image registration(dir) in three temporal and one spatial dimensions through a linear polynomial fitting model, and then use principal component analysis (pca) to decompose the fitted dvfs into a linear combination of the main motion basis to represent conventional respiratory motion. The "Synthetic" ct image of the selected phase is generated by deforming the reconstructed dvfs with the reference ct 00 image. Preliminary results show that this method has the potential to extract regular breathing movements from patients' 4d ct images, and can recover tumor organs and tissues caused by irregular breathing movements during 4d ct image acquisition. Calculate the correlation coefficients(cc) and mean of five patients. Of all the patients ,at superior-inferior(si), anterior-posterior(ap) and medial-latera(ml) mean values of 0.86 ± 0.02, 0.86 ± 0.02 and 0.86 ± 0.02, respectively.

1. Introduction

Four-dimensional computed tomography (4d ct) has been widely used to monitor patient specific respiratory motion for determining individual safety margin in radiation therapy.[1] Usually, the reconstructed 4d ct images suffer from severe or mild artifacts mainly caused by irregular motion during image acquisition. In recent years, many methods have been produced to reduce or correct motion artifacts, but none of them can be applied to all imaging cases.[2] Therefore, the purpose of this study is to propose a method of principal component analysis (pca) combined with linear polynomial fitting model to model the displacement vector field (dvfs) obtained from deformable image registration (dir).[3] The main goal of this study is to reduce the motion artifacts in 4d ct images.

Image artifacts seriously reduce the quality of ct images, sometimes doctors can't diagnose or cause misdiagnoses, and even lead to medical accidents.[4] Motion artifacts can be suppressed without additional hardware.[5] It is more efficient to process moving artifacts by extracting dvfs from images than other methods.[6] Define the cropping boundary box in the three-dimensional viewing directions: coronal, sagittal and transverse. [7]The voxel size in the three directions is 0.9766mm,0.9766mm ,2mm respectively.

2. Materials and Methods

2.1 Imaging Study

The reconstructed 4d ct images were classified into 10 respiratory stages, of which 0% were corresponding to the final inspiratory phase and 50% to the final exhalation. [8]The imaging parameters are as follows: voltage / current: 120 kv / 290 ma, slice thickness: 2.5 mm, rack rotation: 0.5 s per cycle, reconstruction matrix: 512×512, field of view (fov): $450 \leq 500$ mm.

Table 1 Summary of patient

Patient	Age	Gender	Cancer site	Tumor location	ptv (cm^3)
1	69	m	nsclc	r-l lobe	71.8
2	56	f	sclc	l-l lobe	107.0
3	76	f	nsclc	l-u lobe	67.8
4	43	m	nsclc	r-l lobe	964.6
5	54	f	sclc	r-u lobe	71.9
6	60	m	nsclc	l-l lobe	46.0
7	35	m	Sclc	l-u lobe	192.6
8	44	m	nsclc	r-l lobe	72.3
9	45	f	sclc	r-l lobe	457.0
10	73	f	nsclc	l-l lobe	92.4

Abbreviation: m, male; f, female; nsclc, non-small cell lung cancer; sclc, small cell lung cancer; r-l, right-lower; l-l, left-lower; l-u, left, upper; r-u, right-upper ； ptv, planning target volume.

2.2 4D CT Reconstruction

In order to determine the respiratory signal, each ct image is processed to determine the body outline. body area (ba), which is used as a respiratory substitute in 4d ct technology, is defined as the number of pixels in the body outline. Then, by drawing ba as a function of image acquisition time, a separate respiratory curve is generated at each slice position.[9] The complete respiratory signal is obtained by continuously combining each respiratory curve according to the image acquisition time, and then the low frequency component of the signal is removed, which is caused by the change of anatomical structure. In order to reconstruct the 4d ct, the automatic search algorithm is used to detect the respiratory peak from the complete respiratory signal, and then manual correction is carried out to remove the wrong peak detection.[10] The peak is assigned to 50% of the phase and the rest of the phase is calculated by linear interpolation. If the phase is missing, the nearest phase and the corresponding ct image are used to reconstruct the 4d ct. [11]According to the respiratory phase, the two-dimensional film ct images were recombined into 10 stages. In addition, the first two images in the image series at each slice position are excluded for reconstruction, which allows the ct signal to reach a steady state (that is, a consistent signal). All image processing and data analysis are carried out using internal programs implemented in matlab 2018a.

2.3 Deformable Registration Across 4D CT image

Figurer 1 shows the workflow of generating "synthetic" 4d ct based on linear polynomial fitting model and pca in this study.

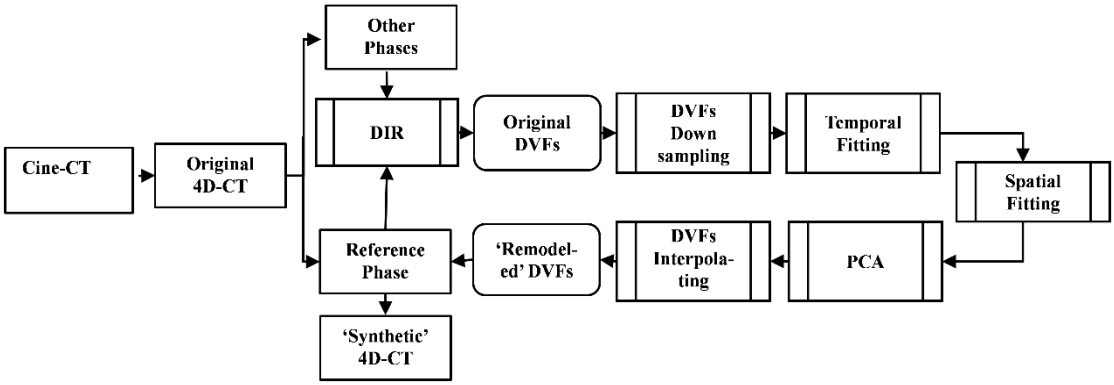

Figure1: Use our method to generate a workflow for synthetic 4d ct.

Firstly, the displacement vector fields (dvfs). Is obtained from the deformable image registration (dir) between the reference-phase image and other images. Secondly, the linear polynomial fitting model is used to fit dvfs into three temporal and spatial dimensions. Thirdly, principal component analysis (pca) is used to decompose each dvfs into linear

combinations based on motion, and its cross subspace is proved to be sufficient to capture the main changes of respiratory motion. Finally, the "synthetic" 4d ct is generated by using the reconstructed dvfs to deform the reference-phase image.[12]

2.4 DVFS Reconstruction

In this study, the obtained dvfs is optimized to solve the artifacts existing in the 4d ct image, and all phase images are transformed into reference images (t = 0%) to calculate the dvfs. Considering the entire pixel during the 4d ct registration process. The displacement continuity at the corresponding phase throughout the breathing cycle uses a linear polynomial fitting model to fit the displacement trajectory of each pixel.[13] Then use the same polynomial to fit the displacement of each phase at adjacent pixels in the three spatial dimensions of x, y and z to correct the potential discontinuous motion introduced by time fitting, so the obtained dvfs(f) and The corresponding time fitting (ft) and space fitting (fs) calculation formulas are:

$$f = \lambda f_t + (1 - \lambda) f_s \tag{1}$$

For two images i and j, while i is the moving image (or reference image) and j is the fixed image (or target image), deformable image registration is to computed the deformation vector field v in order to optimize the system energy equation:[14]

$$e = \int_{\Omega} s(v(i), j) d\Omega + \alpha^2 \int_{\Omega} r(v) d\Omega \tag{2}$$

Where v is the deformation vector field, also commonly referred to as the playground, light flow, etc. v(i) is the deformed motion image i, s is the similarity function, r is the smoothness constraint function, the s is the image domain, and α is a constant.

Determines that motion images and fixed images are matched and calculated. The most important difference between the two sports fields is that the backward sports field is moving the sports field backwards is defined on the voxels of the fixed image, define a forward motion field on a voxel of a moving image

Linear model polynomial:

$$f(x) = p_1 * x\hat{}n + p_2 * x\hat{}(n-1) + p_3 * x\hat{}(n-2) + p_4 * x\hat{}(n-3) \ldots + p_{(n-1)} * x\hat{}2 + p_n *\hat{} \; x + p_{(n+1)} \tag{3}$$

2.2 Reduce Artifacts In 4D CT Images

After the operation of fitting dvfs with covariance, mean variance, eigenvalue eigenvector and so on, it is found that its three eigenvalues can be used to represent its main motion.

The principal component analysis (pca) was used in this study to inhibit or replace artifacts and errors in motion-independent dvfs. The relationship between the dvfs at time t and the number of voxels n is:[15]

$$u(t) = [\sum_{1}^{n} \vec{u}_i(t)]^T \tag{4}$$

Because it is fitted in the three spatial dimensions of x, y and z, the $\vec{u}_i(t)$ of each voxel can be decomposed into:

$$\vec{u}_i(t) = \vec{u}_{i_x}(t) + \vec{u}_{i_y}(t) + \vec{u}_{i_z}(t) \tag{5}$$

Combine formula (4) and formula (5) and transform into[14]:

$$u(t)=[\sum_{1}^{n}\vec{u}_{i_x}(t)]+[\sum_{1}^{n}\vec{u}_{i_y}(t)]+[\sum_{1}^{n}\vec{u}_{i_z}(t)] \tag{6}$$

Calculate the covariance matrix of the fitted dvfs in the three directions of x, y and z the formula is:

$$\begin{aligned} cov &= cov_x + cov_y + cov_z \\ cov_x &= \frac{-1}{n-1}\sum_{1}^{n}(\vec{d'}(i)-\vec{d})\,(\vec{d'}(i)-\vec{d})^T \end{aligned} \tag{7}$$

Where $\vec{d'}$ denotes the fitted column vectors between phase image and reference image and vector $\vec{d}$ denotes the average of these column vectors.

Covx, covy and covz represent the covariance in the x, y and z direction, respectively. Similarly, we can get covy and covz.

In this study, three main motion bases and corresponding projection coefficients are used to reconstruct the original fitting dvfs in each direction, thus the complexity can be significantly reduced without losing the main motion information.

3. Results

We get near real-time images from cine-ct images. We take the trajectory of the lung model determined by the cine-ct image as the basic fact and compare with the model obtained by 4d ct.

Use matlab software to match reference images and other images, select ct 00 as the reference image, and other images as motion images. Refactoring dvfs using linear polynomial fit models and pca, using "synthetic" dvfs to reconstruct 4d ct images.

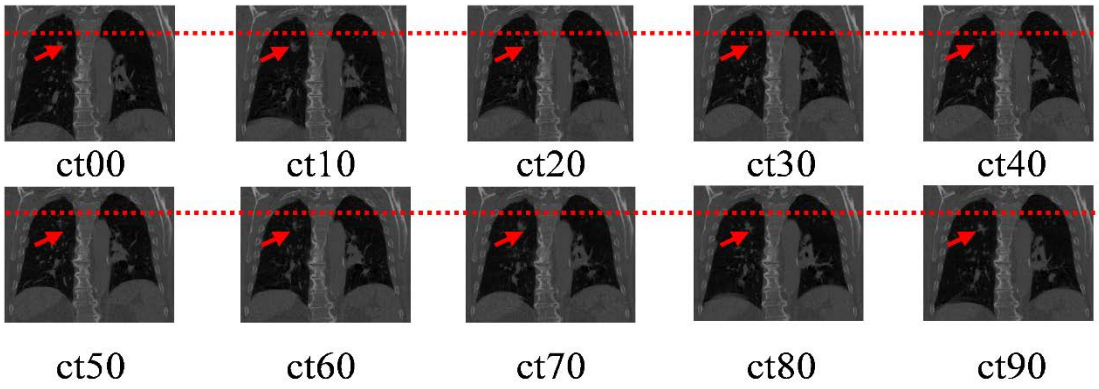

Figure 2: 4d ct Display Example. From the tumor movement of ct00-ct90 indicated by the red arrow, the tumor movement in the whole respiratory cycle can be seen from the dotted line.

Figureure3 show comparison of tumor motion trajectories from cine-ct and ‘synthetic’ 4d ct in three orthogonal directions (*si*, *ap*, and *ml*).

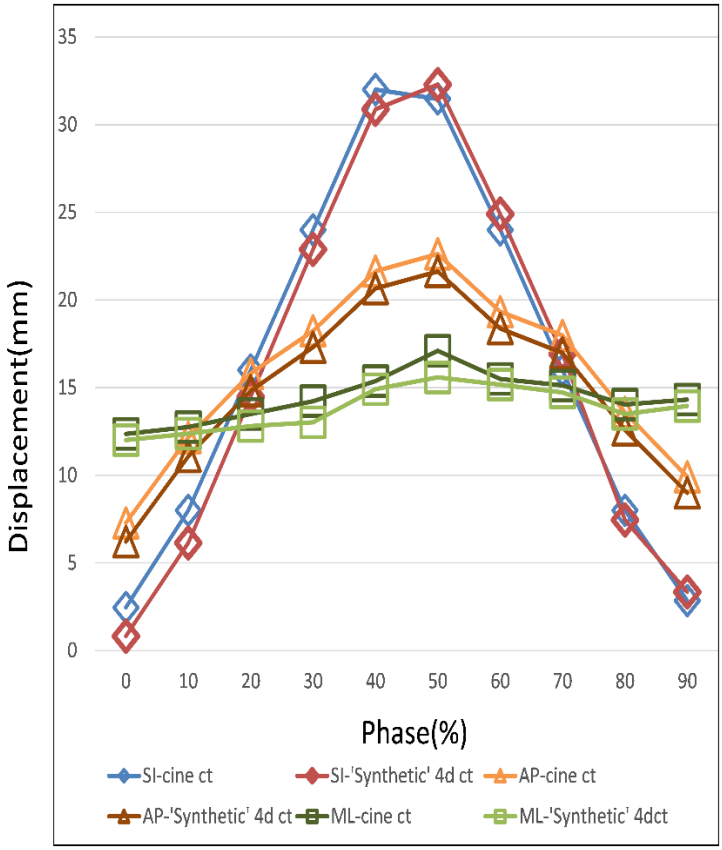

Figure 3: From the patient's starting inhale to the end of the exhalation is a breathing cycle, the entire breathing cycle is divided into ten phases (00-90). We take 40 for the breathing end 90 for the end of the exhalation.

Figureure 4 show the comparison of dvfs in the target face and before fitting after processing with the pca method using linear fit. From the red mark of Figureure 3(a) we can see that the dvfs before processing has obvious motion artifacts, after linear fitting and principal component analysis model processing can be seen from Figureure 3(b) motion artifacts have been basically eliminated.

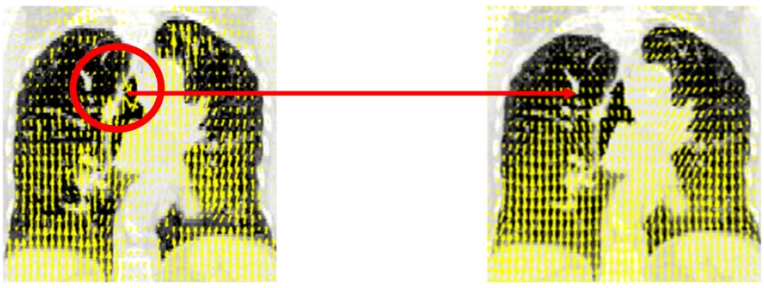

(a) (b)

FIGURE4: Use linear polynomial and principal component analysis (pca) models to compare dvfs on a target face for specific slices before and after processing.

We analyzed five patients' 'synthetic' ct and cine-ct to obtain their correlation coefficients(cc) in three orthogonal directions(si,ap and ml).

Table 2 Measurements for some patients

Number	Age	Gender	Correlation coefficients(cc)								
			SI			AP			ML		
1	69	m	0.86	0.86	0.86	0.88	0.89	0.87	0.85	0.86	0.84
			0.87	0.86	0.84	0.87	0.88	0.85	0.87	0.88	0.87
			0.88	0.84	0.87	0.86	0.85	0.87	0.86	0.84	0.87
2	76	f	0.88	0.86	0.88	0.87	0.84	0.87	0.85	0.84	0.86
			0.79	0.88	0.84	0.86	0.88	0.84	0.87	0.86	0.88
			0.83	0.85	0.84	0.90	0.87	0.84	0.84	0.86	0.85
3	43	m	0.87	0.89	0.86	0.85	0.86	0.87	0.84	0.83	0.86
			0.86	0.84	0.86	0.81	0.83	0.86	0.84	0.82	0.85
			0.87	0.86	0.87	0.89	0.88	0.86	0.87	0.86	0.83
4	60	m	0.86	0.84	0.86	0.87	0.85	0.84	0.82	0.87	0.89
			0.86	0.87	0.86	0.83	0.89	0.87	0.83	0.88	0.85
			0.87	0.87	0.84	0.86	0.83	0.85	0.88	0.87	0.85
5	45	f	0.88	0.93	0.89	0.86	0.91	0.86	0.84	0.86	0.87
			0.86	0.89	0.87	0.88	0.89	0.91	0.88	0.86	0.89
			0.89	0.87	0.89	0.87	0.88	0.86	0.88	0.87	0.86
Mean	/	/	0.87	0.88	0.87	0.87	0.87	0.86	0.84	0.86	0.86
			0.85	0.87	0.85	0.85	0.87	0.87	0.86	0.86	0.87
			0.87	0.86	0.86	0.88	0.86	0.86	0.87	0.86	0.85

Table2: Correlation coefficients(*cc*) and mean for five patients in three orthogonal directions (*si*,*ap* and *ml*)

4. Summary

In this work, we used a mathematical method that combines linear polynomial fiting models with master component analysis, which is mainly used to reduce motion artifacts in 4d ct images. We compared the motion trajectory of the original 4d ct image with the synthetic 4d ct image to verify the motion accuracy of the “synthetic” 4d ct image, and the results show that the proposed method can be used to reduce motion artifacts without losing the information of breathing movement.

References

[1] K. Harada, N. Katoh, R. Suzuki, et al. "Evaluation of the motion of lung tumors during stereotactic body radiation therapy (SBRT) with four-dimensional computed tomography (4DCT) using real-time tumor-tracking radiotherapy system (RTRT)," Physica Medica, vol. 32 (2016) No. 2, p. 305-311.

[2] L. Parkes, B. Fulcher, M. Yücel and A. Fornito "An evaluation of the efficacy, reliability, and sensitivity of motion correction strategies for resting-state functional MRI," Neuroimage, vol. 171 (2018) p. 415-436.

[3] D. Granato, J. S. Santos, G. B. Escher, B. L. Ferreira and R. M. Maggio "Use of principal component analysis (PCA) and hierarchical cluster analysis (HCA) for multivariate association between bioactive compounds and functional properties in foods: A critical perspective," Trends in food science & technology, vol. 72 (2018) p. 83-90.

[4] G. Ragab, M. Elshahaly and T. Bardin "Gout: an old disease in new perspective–a review," Journal of advanced research, vol. 8 (2017) No. 5, p. 495-511.

[5] I. Klovatch-Podlipsky, T. Gazit, F. Fahoum, et al. "Dual array EEG-fMRI: an approach for motion artifact suppression in eeg recorded simultaneously with fMRI," Neuroimage, vol. 142 (2016) p. 674-686.

[6] .S. Zhi, B. Jiang, M. Kachelrieß and X. Mou, "Artifacts reduction method in 4DCBCT based on a weighted demons registration framework," in 15th International Meeting on Fully

Three-Dimensional Image Reconstruction in Radiology and Nuclear Medicine, 2019, vol. 11072, p. 110722R: International Society for Optics and Photonics.

[7] E. Ramasamy, O. Avci, B. Dorow, et al. "An efficient modelling-simulation-analysis workflow to investigate stump-socket interaction using patient-specific, three-dimensional, continuum-mechanical, finite element residual limb models," Frontiers in bioengineering and biotechnology, vol. 6 (2018).

[8] .N. Myziuk, T. Guerrero, G. Sakthivel, et al. "Pulmonary blood mass dynamics on 4DCT during tidal breathing," Physics in Medicine & Biology, vol. 64 (2019) No. 4, p. 045014.

[9] .U. Yoruk, M. Saranathan, A. M. Loening, B. A. Hargreaves and S. S. Vasanawala "High temporal resolution dynamic MRI and arterial input function for assessment of GFR in pediatric subjects," Magnetic resonance in medicine, vol. 75 (2016) No. 3, p. 1301-1311.

[10] J. C. Sanders, P. Ritt, T. Kuwert, A. H. Vija and A. K. Maier "Fully automated data-driven respiratory signal extraction from SPECT images using Laplacian eigenmaps," IEEE transactions on medical imaging, vol. 35 (2016) No. 11, p. 2425-2435.

[11] .C. Zhao, Y. Zhong, X. Duan, et al. "4D cone-beam computed tomography (CBCT) using a moving blocker for simultaneous radiation dose reduction and scatter correction," Physics in Medicine & Biology, vol. 63 (2018) No. 11, p. 115007.

[12] .D. O'Connell, "Development, validation, and translation of a respiratory motion model-based 4DCT technique for use as a clinical protocol for radiation therapy treatment planning," UCLA, 2018.

[13] K. Kuroda "MR techniques for guiding high-intensity focused ultrasound (HIFU) treatments," Journal of Magnetic Resonance Imaging, vol. 47 (2018) No. 2, p. 316-331.

[14] .K. A. Eppenhof, M. W. Lafarge, P. Moeskops, M. Veta and J. P. Pluim, "Deformable image registration using convolutional neural networks," in Medical Imaging 2018: Image Processing, 2018, vol. 10574, p. 105740S: International Society for Optics and Photonics.

[15] M. A. Motin, C. K. Karmakar and M. Palaniswami "Ensemble empirical mode decomposition with principal component analysis: A novel approach for extracting respiratory rate and heart rate from photoplethysmographic signal," IEEE journal of biomedical and health informatics, vol. 22 (2017) No. 3, p. 766-774.